Jefferson Lab PAC20

Proposal Cover Sheet

This document must be received by close of business Thursday,

May 31, 2001 at:

Jefferson Lab
User Liaison,
Mail Stop 12B
12000 Jefferson Ave.
Newport News, VA
23606

Experimental Hall: A

Days Requested for Approval: 35

❒ Proposal Title:

Measurement of the Neutron d_2^n Matrix Element: A linear Combination of the Electric χ_E and Magnetic χ_B Color Polarizabilities

Proposal Physics Goals

Indicate any experiments that have physics goals similar to those in your proposal.

Approved, Conditionally Approved, and/or Deferred Experiment(s) or proposals:

E94-010, E97-103, E99-117, E01-012 and E01-006

Contact Person

Name: Zein-Eddine Meziani
Institution: Temple University
Address: Department of Physics, Barton Hall A323
Address: 1900 North 13th Street
City, State, ZIP/Country: Philadelphia, PA, 19122/USA
Phone: (215) 204-5971 Fax: (215) 204-2569
E-Mail: meziani@unix.temple.edu

Jefferson Lab Use Only

Receipt Date:_____

By:_____

BEAM REQUIREMENTS LIST

JLab Proposal No.: _____ Date: _____

Hall: A Anticipated Run Date: _____ PAC Approved Days: _____

Spokesperson: X. Jiang, Z.-E. Meziani Hall Liaison: J. P. Chen
Phone: (215) 204 5971, (757) 269 7011
E-mail: meziani@unix.temple.edu

List all combinations of anticipated targets and beam conditions required to execute the experiment. (This list will form the primary basis for the Radiation Safety Assesment Document (RSAD) calculations that must be performed for each experiment.)

Condition No.	Beam Energy (MeV)	Mean Beam Current (μA)	Polarization and Other Special Requirements (e.g., time structure)	Target Material (use multiple rows for complex targets — e.g., w/windows)	Material Thickness (mg/cm^2)	Est. Beam-On Time for Cond. No. (hours)
1	6000.	15.	Polarization 80%	^{3}He	50	145
	6000.	15.		Glass window	44	
2	5700.	15.	Polarization 80%	^{3}He	50	641
	5700.	15.		Glass window	44	

The beam energies, E_{Beam}, available are: $E_{Beam} = N \times E_{Linac}$ where N = 1, 2, 3, 4, or 5. $E_{Linac} = 800$ MeV, i.e., available E_{Beam} are 800, 1600, 2400, 3200, and 4000 MeV. Other energies should be arranged with the Hall Leader before listing.

HAZARD IDENTIFICATION CHECKLIST

JLab Proposal No.: E-01-111 Date: 5/31/2001

(For CEBAF User Liaison Office use only.)

Check all items for which there is an anticipated need.

Cryogenics
_____ beamline magnets
_____ analysis magnets
_____ target
type: _____
flow rate: _____
capacity: _____

Electrical Equipment
_____ cryo/electrical devices
_____ capacitor banks
_____ high voltage
_____ exposed equipment

Radioactive/Hazardous Materials
List any radioactive or hazadorous/ toxic materials planned for use:
_____
_____
_____
_____

Pressure Vessels
19 mm inside diameter
13 atm operating pressure
Glass window material
~100 μm window thickness

Flammable Gas or Liquids
type: _____
flow rate: _____
capacity: _____

Drift Chambers
type: _____
flow rate: _____
capacity: _____

Other Target Materials
___ Beryllium (Be)
___ Lithium (Li)
___ Mercury (Hg)
___ Lead (Pb)
___ Tungsten (W)
___ Uranium (U)
X Other (list below)
^{3}He, N_2 and Rb
_____

Vacuum Vessels
_____ inside diameter
_____ operating pressure
_____ window material
_____ window thickness

Radioactive Sources
_____ permanent installation
_____ temporary use
type: _____
strength: _____

Large Mech. Structure/System
_____ lifting devices
_____ motion controllers
_____ scaffolding or
_____ elevated platforms

Lasers
type: Laser diode system
wattage: 7x30 W
class: IV

Installation:
X permanent*
_____ temporary
* for this experiment

Use:
_____ calibration
_____ alignment

Hazardous Materials
____ cyanide plating materials
____ scintillation oil (from)
____ PCBs
____ methane
____ TMAE
____ TEA
____ photographic developers
____ other (list below)
_____
_____

General:
Experiment Class:

X Base Equipment
_____ Temp. Mod. to Base Equip.
_____ Permanent Mod. to Base Equipment
_____ Major New Apparatus

Other: Polarized ^{3}He target with Laser Hut

Measurement of the Neutron d_2^n Matrix Element: A Linear Combination of the Electric χ_E and Magnetic χ_B Color Polarizabilities

P. Bertin
Université Blaise Pascal De Clermont-Ferrand, Aubiere 63177, France

J.-P. Chen, E. Chudakov, C. W. de Jager, J. Gomez, O. Hansen, J. LeRose, N. Liyanage, R. Michaels, S. Nanda, A. Saha, B. Reitz, B. Wojtsekhowski
Jefferson Lab, Newport News, VA 23606, USA

A.T. Katramatou, K. McCormick, G.G. Petratos
Kent State University, Kent, OH 44242

W. Korsch, P. Zolnierczuk
University of Kentucky, Lexington, KY 40506, USA

W. Bertozzi, Z. Chai, S. Gilad, D.W. Higinbotham, M. Rvachev, S. Sirca, Y. Xiao, X. Zheng, J. Zhou and Z. Zhou
Massachusetts Institute of Technology, Cambridge, MA 02139, USA

F. Benmokhtar, S. Dieterich, R. Gilman, C. Glashausser, X. Jiang (Spokesperson), G. Kumbartzki, R. Ransome, S. Strauch
Rutgers University, Piscataway, NJ 08855, USA

Seonho Choi, A. Lukhanin, Z.-E. Meziani (Spokesperson), K. Slifer, P. Solvignon
Temple University, Philadelphia, PA 19122, USA

S. Binet, G. Cates, A. Deur, J. Singh, A. Tobias
University of Virginia, Charlottesville, VA 22901, USA

T. Averett, J. M. Finn, D. Armstrong, K. Griffioen, K. Kramer V. Sulkosky, X. Zhu, J. Roche
College of William and Mary, Williamsburg, VA 23185, USA

and the

Hall A Collaboration

June 2, 2001

Contact: Z.-E. Meziani (meziani@unix.temple.edu)

Abstract

We propose to make a measurement of the spin-dependent scattering cross section for a longitudinally polarized electron beam off a transversely and longitudinally polarized ^{3}He target. The measurement will cover excitation energies across the resonance and deep inelastic regions at constant 4-momentum transfer $Q^2 = 2$ (GeV/c)^2. We will extract the linear combination $2g_1 + 3g_2$ of spin structure functions and evaluate the neutron d_2^n matrix element. This measurement will significantly improve the precision of the neutron d_2^n world data and test the predictions of several models including the updated lattice QCD calculation of this quantity. The matrix element d_2^n reflects the response of the color electric and magnetic fields to the polarization of the nucleon. Because d_2^n is a higher moment of a special linear combination of g_1^n and g_2^n it is dominated by the contributions from the large x region. CEBAF at Jefferson Lab is ideal to perform such a measurement. Since the quantity of interest is an integral we expect that the uncertainty on the nuclear corrections applied in the extraction of the neutron quantity from ^{3}He will not spoil the result at the present stage of statistical precision.

1 Introduction and Motivation

In inclusive polarized lepton-nucleon deep-inelastic scattering, one can access two spin-dependent structure functions of the nucleon, g_1 and g_2. While g_1 can be understood in terms of the Feynman parton model which describes the scattering in terms of *incoherent* parton scattering, g_2 cannot. Rather, one has to consider parton correlations initially present in the participating nucleon, and the associated process is a *coherent* parton scattering in the sense that more than one parton takes part in the scattering. Indeed, using the operator product expansion (OPE) [1, 2], it is possible to interpret the g_2 spin structure function beyond the simple quark-parton model, in terms of the technical jargon in QCD, g_2 is a higher-twist structure function. As such, it is exceedingly interesting because it provides a unique opportunity to study the quark-gluon correlations in the nucleon which cannot otherwise be accessed.

In a recent review Ji [3] explained that higher-twist processes cannot be cleanly separated from the leading twist because of the so-called infrared renormalon problem first recognized by t' Hooft. This ambiguity arises from separating quarks and gluons pre-existing in the hadron wave function from those produced in radiative processes. Such a separation turns out to be always scheme dependent. Nevertheless, the g_2 structure function is an **exception** because it contributes at the leading order to the spin asymmetry of longitudinally-polarized lepton scattering on transversely-polarized nucleons. Thus, g_2 is among the *cleanest* higher-twist observables.

Why does the g_2 structure function contain information about the quark and gluon correlations in the nucleon? According to the optical theorem, g_2 is the imaginary part of the spin-dependent Compton amplitude for the process $\gamma^*(+1) + N(1/2) \to \gamma^*(0) + N(-1/2)$,

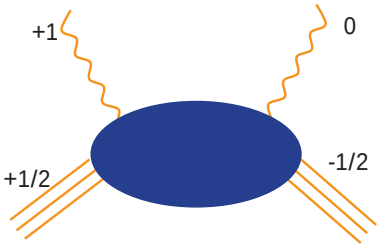

Figure 1: Compton amplitude of $\gamma^*(+1) + N(1/2) \to \gamma^*(0) + N(-1/2)$.

where γ^* and N denote the virtual photon and the nucleon, respectively, and the numbers in the brackets are the helicities. Thus this Compton scattering involves the t-channel helicity exchange $+1$. When it is factorized in terms of parton sub-processes, the intermediate partons must carry

this helicity exchange. Because of the chirality conservation in vector coupling, massless quarks in perturbative processes cannot produce a helicity flip. Nevertheless, in QCD this helicity exchange may occur in the following two ways (see Fig. 2): first, single quark scattering in which the quark carries one unit of orbital angular momentum through its transverse momentum wave function; second, quark scattering with an additional transversely-polarized gluon from the nucleon target. The two mechanisms are combined in such a way to yield a gauge-invariant result. Consequently, g_2 provides a direct probe of the quark-gluon correlations in the nucleon wave function.

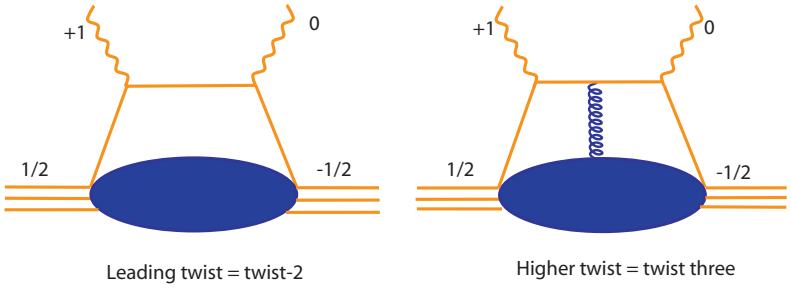

Figure 2: Twist-two and twist-three contributions to Compton scattering

The piece of interesting physics we want to focus on in this proposal contains the second moment in x of a linear combination of g_1 and g_2,

$$d_2(Q^2) = a_2(Q^2) + 3\int_0^1 x^2 g_2(x,Q^2)dx \quad (1)$$

$$= 2\int_0^1 x^2 g_1(x,Q^2)dx + 3\int_0^1 x^2 g_2(x,Q^2)dx \quad (2)$$

where $a_2(Q^2)$ is a twist-two matrix element related to the second moment of the $g_1(x)$ structure function. The $d_2(Q^2)$ matrix element is a twist-three matrix element which is related to a certain quark gluon correlation,

$$\langle PS|\frac{1}{4}\bar{\psi}g\tilde{F}^{\sigma(\mu}\gamma^{\nu)}\psi|PS\rangle = 2d_2 S^{[\sigma}P^{(\mu]}P^{\nu)} \ , \quad (3)$$

where $\tilde{F}^{\mu\nu} = (1/2)\epsilon^{\mu\nu\alpha\beta}F_{\alpha\beta}$, and $(\cdots)$ and $[\cdots]$ denote symmetrization and antisymmetrization of indices, respectively. The structure of the above operator suggests that it measures a quark *and* a gluon amplitude in the initial nucleon wavefunction [1, 2].

The significance of $d_2(Q^2)$ has been articulated by Ji and we quote, "*we ask when a nucleon is polarized in its rest frame, how does the gluon field inside of the nucleon respond? Intuitively, because of the parity conservation, the color magnetic field* $\vec{B}$ *can be induced along the nucleon polarization and the color electric field* $\vec{E}$ *in the plane perpendicular to the polarization*". After introducing the color-singlet operators $O_B = \psi^\dagger g\vec{B}\psi$ and $O_E = \psi^\dagger\vec{\alpha}\times g\vec{E}\psi$, we can define the gluon-field polarizabilities χ_B and χ_E in the rest frame of the nucleon,

$$\langle PS|O_{B,E}|PS\rangle = \chi_{B,E}2M^2\vec{S} \ . \quad (4)$$

Then d_2 can be written as

$$d_2 = (2\chi_B + \chi_E)/3 \ . \quad (5)$$

Thus d_2 is a measure of the response of the color electric and magnetic fields to the polarization of the nucleon.

2 Experimental Situation for $d_2^{n,p}$ Matrix Elements

The early measurements of the g_2 spin structure function performed by the SMC [4] and E142 [5, 6] collaborations in the 90's were meant to reduce the systematic errors when extracting g_1 due to g_2's contribution in the measured parallel asymmetries. As the statistical precision of g_1 improved a better measurement of g_2 was required to minimize the error on g_1. E143 [7], E154 [8] and E155 [9] collaborations evaluated d_2 and published their results. It is only recently that a dedicated experiment, known as the SLAC E155X [10] was performed to measure g_2 with much improved statistical precision on the proton and the deuteron [11]. Presently the precision of the world data on g_2 is dominated by E155X (see Fig. 3) which has improved the statistical precision over previous experiments by a factor of three.

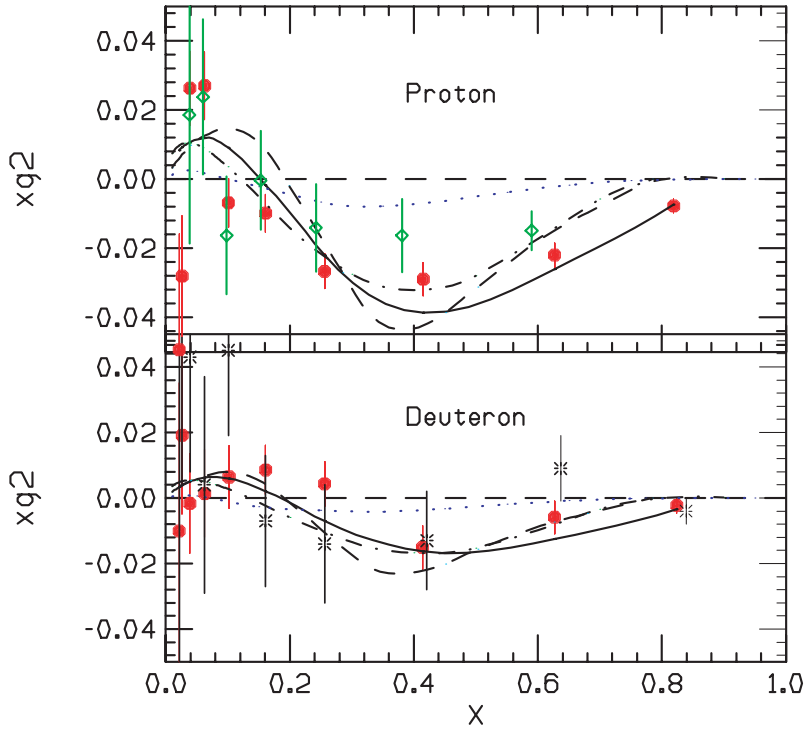

Figure 3: Preliminary E155X results (filled circles) for xg_2^p (top panel) and xg_2^d (bottom panel) compared to xg_2^{WW} (solid line), and several nucleon models; a bag model of Stratmann (dot-dashed line), a chiral soliton model of Weigel *et. al.* (dashed line) and a relativistic bag model of Song (dotted line) (see text for references). SLAC E143 (proton) at 29 GeV and SLAC E155 at 38 GeV (deuteron) results are represented by the diamonds and stars respectively

The precision of the proton measurement of g_2 spin structure function is consistent with g_2^{WW} [15] (the leading twist contribution evaluated using the world fit to the g_1 structure function data) , the bag model calculation of Stratmann [19] and the chiral soliton model of Weigel *et al.* [18]. However, it clearly disagrees with the center-of-mass bag model of Song [21]. From those experimental results we can safely say that higher twist effects are small for the proton. While a comparison of the x dependence of g_2 with a calculation based on fundamental principles like that of Lattice QCD is not possible, the d_2 matrix element offers a unique opportunity for such comparison at this stage of statistical precision. Our ultimate interest lies on a direct comparison of the second moment of $(3g_2 + 2g_1)$ with the lattice QCD calculations.

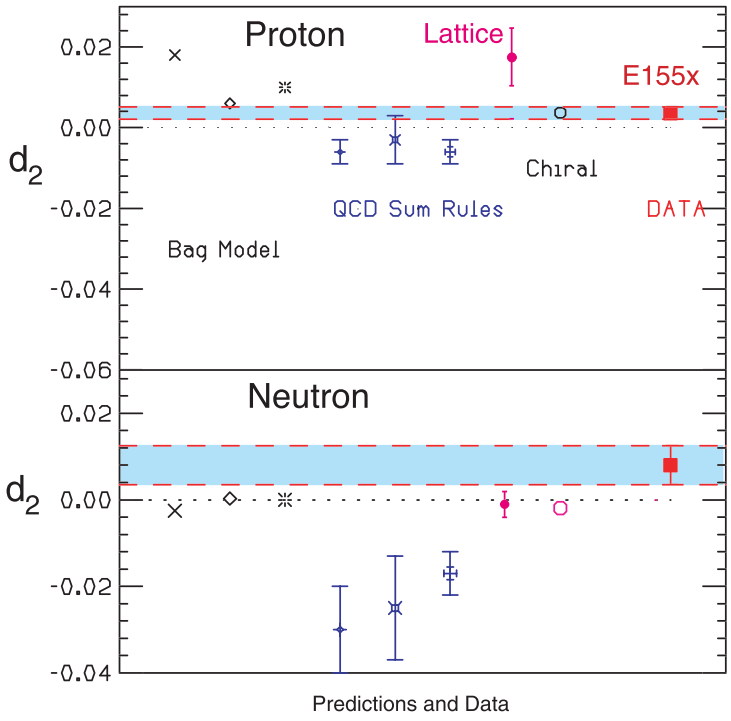

Figure 4: Preliminary E155X results of the nucleon d_2 matrix element compared to several theoretical calculations (see text). Upper panel is for the proton and lower panel for the neutron.

Fig. 4 shows preliminary results of the SLAC E155X d_2 matrix element compared to several calculations. For the proton the results are generally consistent with the chiral quark model [18]and some bag models [19, 20, 22] while one to two standard deviations away from the QCD sum rule calculations [23, 24, 25]. The comparison with the lattice QCD calculation [27] is promising but the error bar on this calculation is still large. The situation for the proton clearly poses a challenge to the theoretical approaches based on fundamental principles of QCD. The Lattice Hadron Collaboration based at Jefferson Lab has plans to calculate this matrix element for the proton and the neutron [12].

For the neutron the situation is less clear since most models predict values consistent with a negative value or zero while the experimental result is positive and 2σ away from zero. Since g_2^n in these models is negative at large x it is conceivable that the poor precision (Fig. 5) of the data in this region is affecting the overall sign of the result. It is important to note that from the point of view of a simple quark model, the d_2 matrix element of the neutron should be much smaller than that of the proton because of SU(6) spin-flavor symmetry. Therefore with the present precision of E155x neutron data it is difficult to draw any conclusions on the sign and size of the neutron higher twist (twist-tree) contribution. Because the d_2 matrix element is a second moment in x of the linear combination $(2g_1 + 3g_2)$ the situation for the neutron can be improved significantly at Jefferson Lab. Fortunately, because of the x^2 weighting, we do not need very precise data at very small x and can use the world existing and future data in the region $x < 0.24$.

As an important first step JLab experiment E97-103 [13], scheduled to run this summer, will provide a precision measurement of g_2^n in the deep inelastic region at low x $(0.17 < x < 0.21)$ and will investigate its Q^2 evolution in the range $0.56 < Q^2 < 1.4$ (GeV^2) for a fixed value of $x \approx 0.2$. The unprecedented statistical accuracy expected in E97-103 should allow us to probe the size of higher twists contributions by comparing directly the measured g_2^n to the leading twist

contribution (twist-two contribution known as $g_2^{n(WW)}$ [15]). Two other approved experiments, JLab experiment E01-012 [16] which uses a polarized ^{3}He target and JLab experiment E01-006 [17] which uses polarized NH_3 and ND_3 targets, will add to the wealth of neutron spin structure functions data (g_1^n and g_2^n) but with an emphasis on the g_1 spin structure function.

The neutron result of g_2 extracted from the proton and deuteron measurements of E155X is shown in Fig. 5 along with what is expected from this proposed experiment. While in the case of the proton the bag model of Stratmann [19] and the chiral soliton model of Weigel *et al.* [18] seem to peak at the same value of x (see Fig. 3), it is not the case for the neutron; however in both models the Burkhardt-Cottingham sum rule is fulfilled and the d_2 matrix element values are similar. Our statistical precision at each x value is not good enough for discriminating between these two models but will provide an improvement of a factor of four on the statistical uncertainty of d_2

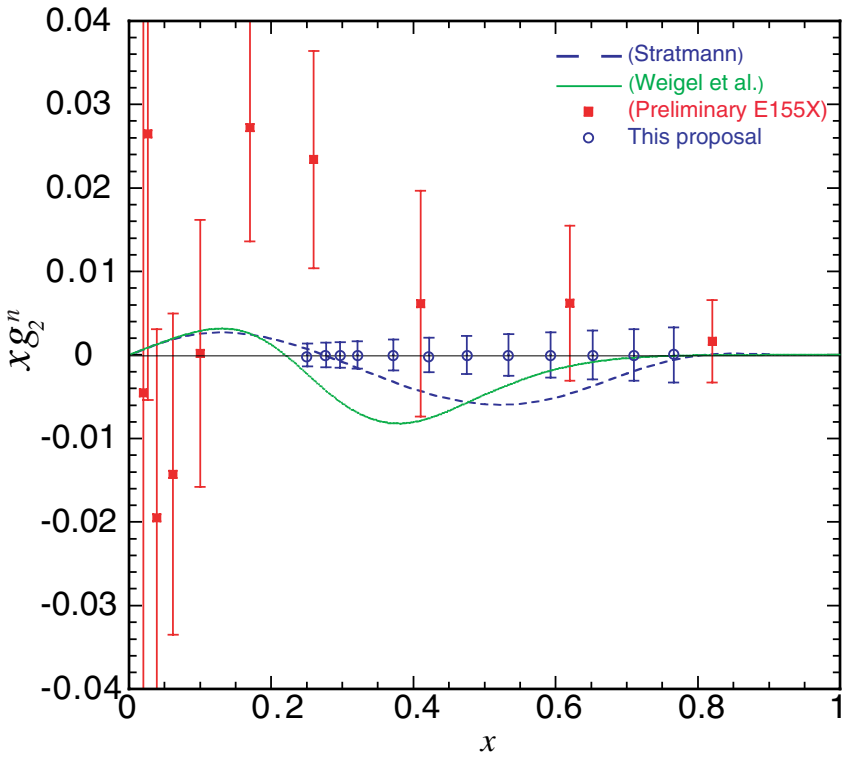

Figure 5: Preliminary E155X results of the xg_2^n extracted by subtracting the proton from the deuteron following the prescription described in Ref.[14]. We also show the resulting statistical error achievable in this proposal on xg_2 with a measurement optimized for d_2. The calculations are those of Stratmann's bag model [19] (dashed line) and Weigel *et. al.*'s chiral soliton model [18] (solid line)

On the experimental side this situation can be improved using a target complementary to polarized deuterium (namely polarized ^{3}He) in order to extract the neutron information. JLab is in a unique position to provide high luminosity to measure the large x region with good statistical precision. Unlike in previous experiments, world data fits of $R = \sigma_L/\sigma_T$, F_2 and g_1 will not be used to evaluate g_2, rather we shall measure absolute polarized cross sections for both directions of the target spin, parallel and perpendicular and extract g_2. Furthermore, in order to evaluate d_2 in those experiments, it is common practice to evolve the measured g_2 data from the measured Q^2

to a common Q^2 value, however, this evolution is not well understood for the twist-tree part of g_2. In contrast, our data will be measured at a constant Q^2.

At large x, the $1/Q^2$ corrections to the twist-three might be important. However, because of the parton-hadron duality, the $1/Q^2$ contribution to the moment is negligible for $Q^2 \geq 2$ GeV^2.

We shall describe in this proposal how CEBAF is in a unique position to improve the neutron measurement of d_2^n by a factor of four.

3 Proposed Experiment

We propose to measure the unpolarized cross section $\sigma_0^{^3He}$, the parallel asymmetry $A_\parallel^{^3He}$ and perpendicular asymmetry $A_\perp^{^3He}$ at a constant Q^2. We will use the longitudinally polarized ($P_b = 0.8$) CEBAF electron beam and a 40-cm-long high pressure polarized ^{3}He target. The measurement will be performed at two incident electron beam energies E_i = 5.7 GeV and 6.0 GeV using both HRS spectrometers at four scattering angles $\theta = 17.5^\circ$, 20.0°, 22.5° and 25.0°. Five momentum settings for each spectrometer will cover the range $0.24 \leq x \leq 0.8$ at Q^2= 2.0 (GeV)^2. The target polarization orientation will be set longitudinal or transverse to the beam with a value of $P_t = 0.40$ while the beam helicity will be reversed at a rate of 30 Hz. A beam current of 15 μA combined with a target density of 2.5×10^{20} atoms/cm^3 provides a luminosity ranging between 5.9×10^{35} cm^{-2}s^{-1} and 8.3×10^{35} cm^{-2}s^{-1} depending on the effective target length at various angles.

3.1 Kinematics

The kinematic settings were chosen to allow a measurement at constant Q^2 over as wide an excitation energy range as possible. Fig. 6 shows in the (Q^2, x) plane the experimental excitation range we plan to cover from the pion threshold to the deep inelastic region including the nucleon resonance region. In order to keep Q^2 constant for each measured x bin, the scattering angle must range from 17.5° to 25°. Then by taking into account the angular acceptance of the HRS spectrometers ($\Delta\theta \approx \pm 25$ mrad) we find a continuous coverage of the x range at constant Q^2 (diamonds of different sizes shown on Fig. 6)

The main contribution to d_2 arises from the large x region because of the weighting of g_1 and g_2 by x^2 in the integration over x. The measurement of this region with high precision is important. In tables 3, 4 and 5 we have listed the kinematical conditions for each spectrometer needed to cover the proposed x region.

3.2 The Polarized Beam

In this proposal we shall assume, that the achievable beam polarization at CEBAF is 80% with a current of $15\mu A$. While about 70% electron beam polarization has been delivered on a regular basis to E94-010 and E95-001 we are optimistic that by the time this experiment runs and with the experience gained using the strained GaAs cathodes, 80% beam polarization will be achieved. The polarization of the beam will be measured with the Hall A Moller and Compton polarimeters.

3.3 The Polarized ^{3}He Target

The polarized target will be based on the principle of spin exchange between optically pumped alkali-metal vapor and noble-gas nuclei [28, 29, 30]. It is the same as that used in JLab experiments E94-010, E95-001 and E97-103 in Hall A.

A central feature of the target will be sealed glass target cells, which under operating conditions, will contain a ^{3}He pressure of about 10 atmospheres. As indicated in Fig. 7, the cells will have

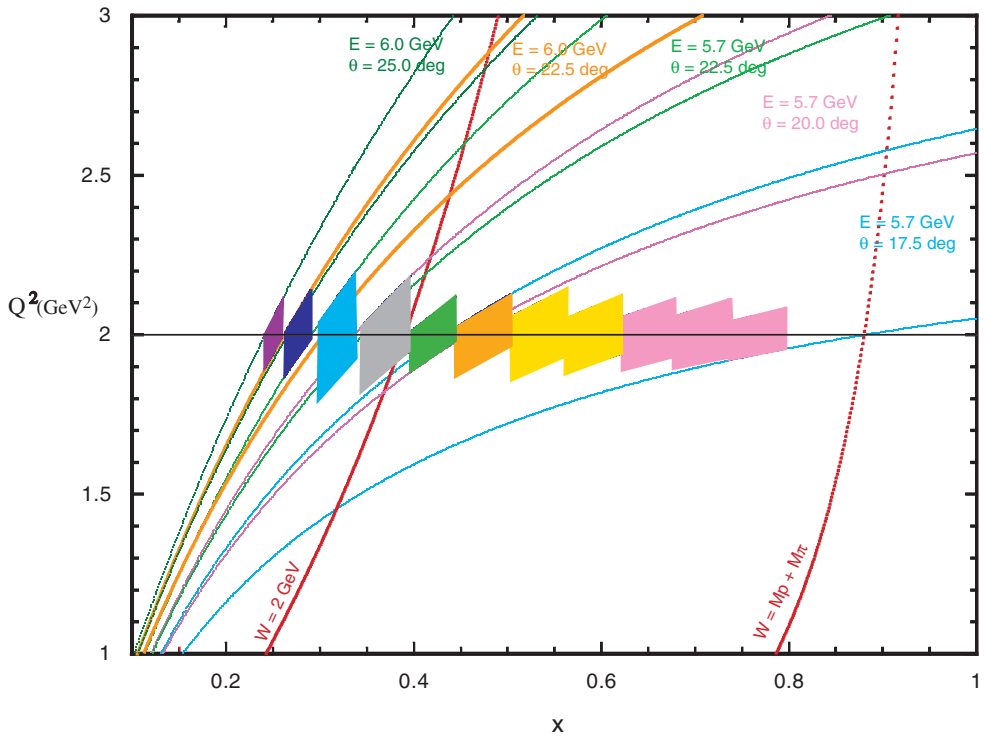

Figure 6: Proposed kinematic range for the measurement at a constant average Q^2 of 2 GeV^2. Each diamond represents the size of an (x,Q^2) bin chosen for this measurement. Each pair of common colored lines is plotted to indicate the possible range of (x,Q^2) due to the angular acceptance of the spectrometer for a fixed incident energy and scattering angle. The electron beam incident energy and the scattering angle and momentum of each spectrometer is chosen to keep the measured data at constant Q^2.

two chambers, an upper chamber in which the spin exchange takes place, and a lower chamber, through which the electron beam will pass. In order to maintain the appropriate number density of the alkali-metal Rubidium the upper chamber will be kept at a temperature of 170–200° using an oven constructed of high temperature plastic Torlon. The density of the target will be about 2.5×10^{20} atoms/cm^3. The lower cell length will be 40 cm such that the end glass windows are not seen by the spectrometer acceptance when it is set at a scattering angle of 17.5° and larger. The effective target thickness will range from 6.0×10^{21} atoms/cm^2 to 8.3×10^{21} atoms/cm^2, since the spectrometer acceptance sees a length of 7 cm/sin θ_e

The main components of the target are shown in Fig. 7. The main "coils" shown are large Helmholtz coils used to apply a static magnetic field of about 25 Gauss. Also shown are the components for the NMR and EPR polarimetry. The NMR components of the target include a set of RF drive coils, and a separate set of pickup coils. Not shown in the figure are the NMR electronics, which include an RF amplifier, a lock-in amplifier, some bridge circuitry, and the capability to sweep the static magnetic field. The EPR components include an EPR excitation coil and a photodiode for detection of the EPR line. The oven shown in Fig. 7 is heated with forced hot air. The optics system include a system of 4 diode lasers for longitudinal pumping and 4 for transverse pumping. A polarizing beam splitter, lens system and a quarter wave plate are required to condition each laser beam line and provide circular polarization.

3.3.1 Operating Principles

The time evolution of the ^{3}He polarization can be calculated from a simple analysis of spin-exchange and ^{3}He nuclear relaxation rates[31]. Assuming the ^{3}He polarization $P_{^3He} = 0$ at $t = 0$,

$$P_{^3He}(t) = P_{Rb} \left(\frac{\gamma_{SE}}{\gamma_{SE} + \Gamma_R} \right) \left(1 - e^{-(\gamma_{SE}+\Gamma_R)\,t} \right) \tag{6}$$

where γ_{SE} is the spin-exchange rate per ^{3}He atom between the Rb and ^{3}He, Γ_R is the relaxation rate of the ^{3}He nuclear polarization through all channels other than spin exchange with Rb, and P_{Rb} is the average polarization of the Rb atoms. Likewise, if the optical pumping is turned off at $t = 0$ with $P_{^3He} = P_0$, the ^{3}He nuclear polarization will decay according to

$$P_{^3He}(t) = P_0\, e^{-(\gamma_{SE}+\Gamma_R)\,t}. \tag{7}$$

The spin exchange rate γ_{SE} is defined by

$$\gamma_{SE} \equiv \langle \sigma_{SE}\ v \rangle\ [Rb]_A \tag{8}$$

where, $\langle \sigma_{SE}\ v \rangle = 1.2 \times 10^{-19}$ cm^3/sec is the velocity-averaged spin-exchange cross section for Rb–^{3}He collisions[31, 32, 33] and $[Rb]_A$ is the average Rb number density seen by a ^{3}He atom. The target operates with $1/\gamma_{SE} = 8$ hours. From equation (6) it is clear that the best possible ^{3}He polarization is obtained by maximizing γ_{SE} and minimizing Γ_R. But from equation (8) we can see that maximizing γ_{SE} means increasing the alkali-metal number density, which in turn means more

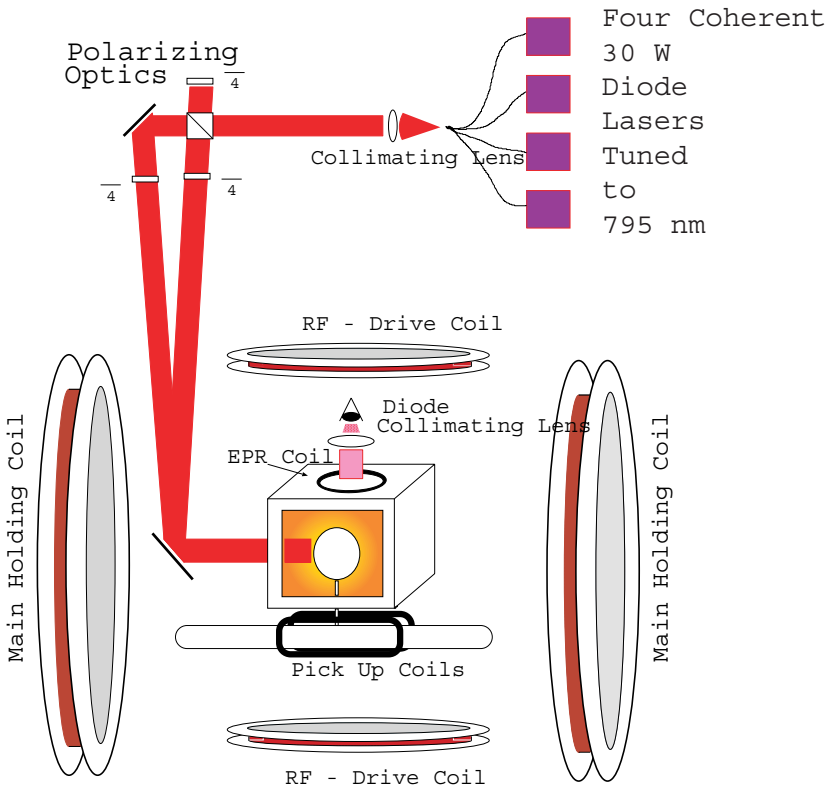

Figure 7: JLab Hall A polarized ^{3}He target setup.

laser power. The number of photons needed per second must compensate for the spin relaxation of Rb spins. In order to achieve $1/\gamma_{\rm SE} = 8$ hours, about 50 Watts of usable laser light at a wavelength of 795 nm will be required.

The rate at which polarization is lost is characterized by Γ and has four principle contributions. An average electron beam current of about 15 μA will result in a depolarization rate of $\Gamma_{beam} = 1/30$ hours [34]. The cells produced in previous experiments typically have an intrinsic rate of $\Gamma_{cell} = 1/50$ hours. This has two contributions, relaxation that occurs during collisions of ^{3}He atoms due to dipole-dipole interactions, and relaxation that is largely due to the interaction of the ^{3}He atoms with the walls. Finally, relaxation due to magnetic field inhomogeneities was held to about $\Gamma_{\nabla B} = 1/100$ hours. Collectively, under operating conditions, we would thus expect

$$\Gamma_R = \Gamma_{beam} + \Gamma_{cell} + \Gamma_{\nabla B} = 1/30\,\text{hours} + 1/50\,\text{hours} + 1/100\,\text{hours} = 1/16\,\text{hours}.$$

Thus, according to equation (6), the target polarization cannot be expected to exceed

$$P_{max} = \frac{\gamma_{\rm SE}}{\gamma_{\rm SE} + \Gamma_{\rm R}} = 0.66$$

Realistically, a Rb polarization of 100% in the pumping chamber will not be achieved, which will reduce the polarization to about 40%.

During E94-010 and E95-001 we achieved a polarization of about 30-35% when a beam current of 15μA was used. The beam depolarization was slightly larger than expected and this was the first time that such a large beam current was used for an extended period time. An R&D effort is underway by JLab and the polarized ^{3}He target collaboration to improve the achievable polarization under the beam conditions proposed in this experiment.

3.3.2 Target Cells

The length of the cell has been chosen to be 40 cm so that the end windows are not within the acceptance of the Hall A spectrometers at angles equal to 17.5° and larger. The end windows themselves will be about 100 μm thick.

3.3.3 The Optics System

As mentioned above, approximately 50 W of "usable" light at 795 nm will be required. By "usable", we mean circularly polarized light that can be readily absorbed by the Rb. It should be noted that the absorption line of Rb has a full width of several hundred GHz at the high pressures of ^{3}He at which we will operate. Furthermore, since we will operate with very high Rb number densities that are optically quite thick, even light that is not well within their absorption line width can still be absorbed.

The laser system is similar to that used in E94-010. It consists of commercially available 30 Watt fiber-coupled diode laser systems (from COHERENT INC.). Four such lasers are used to pump along the transverse direction and three along the longitudinal direction. The efficiency of these lasers has been tested during experiment E94-010 and E95-001 and found to be totally adequate for this experiment's needs.

3.3.4 Polarimetry

Polarimetry is accomplished by two means. During the experiment, polarization is monitored using the NMR technique of adiabatic fast passage (AFP)[35]. The signals are calibrated by comparing the ^{3}He NMR signals with those of water. The calibration is then independently verified by studying the frequency shifts that the polarized ^{3}He nuclei cause on the electron paramagnetic resonance

(EPR) lines of Rb atoms [34]. Both methods were used in E94-010 and we found as expected that the NMR measurements with water calibration are consistent with the EPR results.

3.4 The Spectrometers Setup

We plan to use both HRS spectrometers in Hall A. We will use the right spectrometer with its standard detector package for electrons and the left spectrometer with an added double layer lead glass calorimeter which was first used in E94-010. Each spectrometer will then consist of;

- Two vertical Drift Chambers (VDCs) for the measurement of momentum and production angle.
- Gas Čerenkov counter for pion rejection.
- A set of scintillators for triggering on charged particles.
- A double layer lead glass calorimeter for additional pion rejection.

As the E94-010 analysis shows, the pion rejection factor with the Čerenkov counter and the lead glass calorimeter are better than 2×10^{-4} which is sufficient for our worst case.

Because the maximum momentum attainable by each spectrometer is different (4.30 GeV for the HRS-l and 3.17 GeV for the HRS-r) we have assigned HRS-l to perform the measurements for electron momenta greater than 3 GeV and HRS-r for those measurements with momenta equal or less than 3 GeV. We optimized the time sharing between the two spectrometers (see Table 4 and 5). Although we need to make few spectrometer angle changes to keep our measurement at constant Q^2. Specific advantages make these spectrometers a well matched tool for the proposed measurement.

- Good electron events in the spectrometer are in principle due only to electron scattering off ^{3}He nuclei since the target cell glass windows are outside the spectrometer acceptance. However, excellent target reconstruction by the HRS spectrometers allows for better background rejection.
- An excellent resolution of the spectrometers permits the measurement of elastic scattering off ^{3}He needed for an absolute calibration of the detector in order to measure absolute cross sections.

4 Evaluation of d_2^n Matrix Element

The goal of this experiment is to obtain the d_2 matrix element from the direct measurement of the unpolarized cross section σ_0 and the parallel $A_\parallel$ and perpendicular $A_\perp$ asymmetries on ^{3}He. Equivalently the d_2 matrix element is obtained from the measurement of the linear combination of the spin structure functions $g_1(x,Q^2)$ and $g_2(x,Q^2)$ and forming the second moment of this combination namely,

$$d_2(Q^2) = \int_0^1 x^2[2g_1(x,Q^2) + 3g_2(x,Q^2)]\ dx = \int_0^1 \tilde{d}_2(x,Q^2)\ dx \tag{9}$$

The spin structure functions can be expressed in terms of asymmetries and unpolarized cross sections as follow;

$$g_1 = \frac{MQ^2}{4\alpha^2}\frac{y}{(1-y)(2-y)}2\sigma_0\left[A_\parallel + \tan\frac{\theta}{2}A_\perp\right] \tag{10}$$

$$g_2 = \frac{MQ^2}{4\alpha^2}\frac{y^2}{2(1-y)(2-y)}2\sigma_0\left[-A_\parallel + \frac{1+(1-y)\cos\theta}{(1-y)\sin\theta}A_\perp\right] \tag{11}$$

where σ_0 is the unpolarized cross section, Q^2 is the four momentum transfer, α the electromagnetic coupling constant, θ the scattering angle and $y = (E - E')/E$ the fraction of energy transferred to the target. $A_\parallel$ and $A_\perp$ are the parallel and perpendicular asymmetries,

$$A_\parallel = \frac{\sigma^{\downarrow\Uparrow} - \sigma^{\uparrow\Uparrow}}{2\sigma_0}, \qquad A_\perp = \frac{\sigma^{\downarrow\Rightarrow} - \sigma^{\uparrow\Rightarrow}}{2\sigma_0} \tag{12}$$

From (10), (11) and (12) we can express the integrand of the d_2 matrix element directly in terms of measured asymmetries and unpolarized cross section as follows:

$$\tilde{d}_2(x, Q^2) = x^2[2g_1(x, Q^2) + 3g_2(x, Q^2)] \tag{13}$$

$$= \frac{MQ^2}{4\alpha^2}\frac{x^2y^2}{(1-y)(2-y)}\sigma_0\left[\left(3\frac{1+(1-y)\cos\theta}{(1-y)\sin\theta} + \frac{4}{y}\tan\frac{\theta}{2}\right)A_\perp + \left(\frac{4}{y} - 3\right)A_\parallel\right] \tag{14}$$

The above expression of the integrand is used for the following purposes:

- Determination of the time sharing between the transverse and the longitudinal measurement to minimize the statistical error on d_2 not on g_2 as in previous experiments.
- Determination of the effect of the target polarization orientation misalignment on the systematic error of d_2
- Determination of the systematic error on d_2 due to the systematic errors of the cross section and asymmetries measurements.

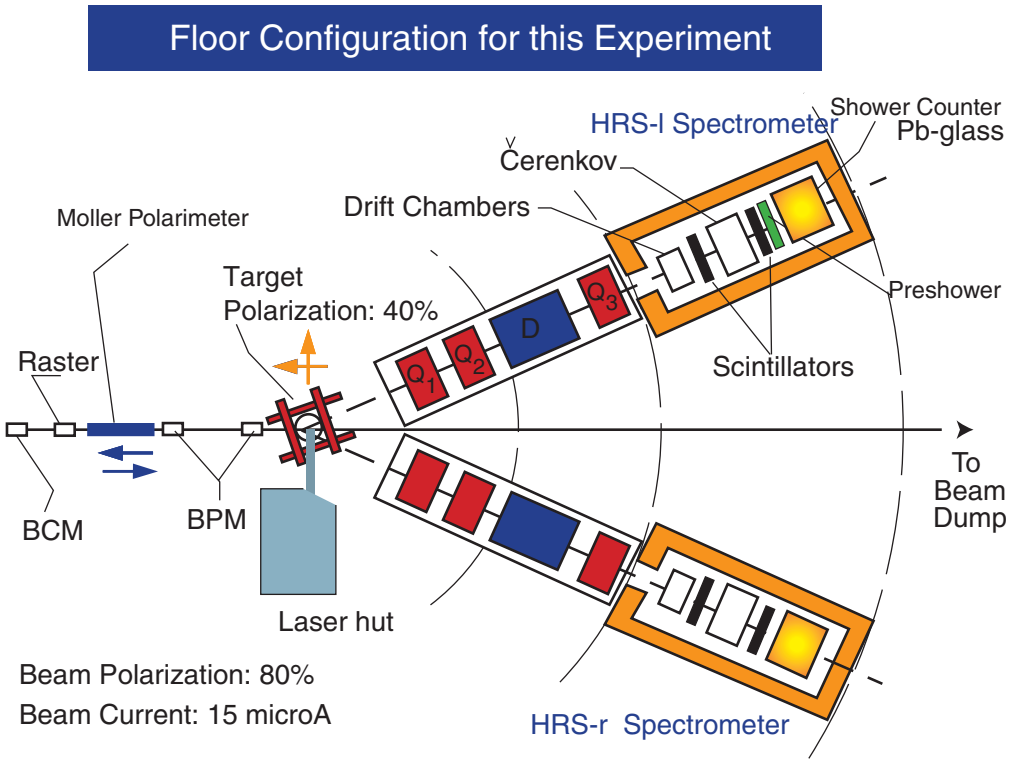

Figure 8: JLab Hall A floor setup using the HRS spectrometers and the polarized 3He target.

The measurement consists of collecting data at two incident energies ($E_i = 5.7$ GeV and 6.0 GeV) and four scattering scattering angles ($\theta = 17.5^\circ, 20.0^\circ, 22.5^\circ$ and 25.0°) and for eight spectrometer momentum settings to cover the range $0.25 \leq x \leq 0.8$. The measured raw ^{3}He counting parallel asymmetry $\Delta_\parallel$ and perpendicular asymmetry $\Delta_\perp$ are converted to the experimental asymmetries $A_\parallel^{^3He}$, and $A_\perp^{^3He}$ respectively, using the relation

$$A_\perp^{^3He} = \frac{\Delta_\perp}{P_b P_t \cos\phi} \qquad A_\parallel^{^3He} = \frac{\Delta_\parallel}{P_b P_t} \tag{15}$$

$$\Delta_\perp = \frac{(N^{\uparrow\Rightarrow} - N^{\uparrow\Rightarrow})}{(N^{\uparrow\Rightarrow} + N^{\uparrow\Rightarrow})} \qquad \Delta_\parallel = \frac{(N^{\downarrow\Uparrow} - N^{\uparrow\Uparrow})}{(N^{\downarrow\Uparrow} + N^{\uparrow\Uparrow})} \tag{16}$$

where $N^{\uparrow\Downarrow}$ ($N^{\uparrow\Uparrow}$) and $N^{\uparrow\Rightarrow}$ ($N^{\uparrow\Rightarrow}$) represent the rate of scattered electrons for each bin in x and Q^2 when the electron beam helicity and target spin are parallel or perpendicular. ϕ is the angle between the scattering plane and the plane formed by the incoming beam and the perpendicular target polarization. $P_b = 0.80$ and $P_t = 0.40$ are the beam and target polarization respectively. The target length (40 cm) is chosen such that no extra dilution of the asymmetry occurs from unpolarized scattering off the glass windows. However, empty target measurements will be performed to insure that no spurious unpolarized background originating in the target area reduces the measured physics asymmetries. The kinematics and electron rates are presented in Table 3. We used the Whitlow 1990 [36] parametrization of unpolarized structure functions from measurements of deep inelastic scattering on the proton and the deuteron. We added incoherently the appropriate structure functions to generate the ^{3}He cross sections. The rates were determined assuming a solid angle evaluated from the bins shown in Fig. 6 and a luminosity varying from 6.0×10^{35} cm^{-2}s^{-1} to 8.0×10^{35} cm^{-2}s^{-1}. The times for the transverse and longitudinal measurements were determined by optimizing the time sharing for the best precision on the integrand $\tilde{d}_2$. If we set

$$\alpha = \frac{MQ^2}{4\alpha^2}\frac{x^2y^2}{(1-y)(2-y)}\sigma_0\left(3\frac{1+(1-y)\cos\theta}{(1-y)\sin\theta} + \frac{4}{y}\tan\frac{\theta}{2}\right) \tag{17}$$

$$\beta = \frac{MQ^2}{4\alpha^2}\frac{x^2y^2}{(1-y)(2-y)}\sigma_0\left(\frac{4}{y} - 3\right) \tag{18}$$

The optimum ratio between the parallel and perpendicular counts is

$$N_\parallel = \frac{\beta}{\alpha}N_\perp \tag{19}$$

The total number of counts $N_\perp$ is given by

$$N_\perp = \frac{\alpha(\alpha+\beta)}{P_b^2 P_t^2 f^2 (\Delta\tilde{d}_2)^2} \tag{20}$$

$f = W_1^n/W_1^{^3He}$ is the fraction of scattering originating from the neutron compared to ^{3}He We required an absolute statistical uncertainty on the integrand $\Delta\tilde{d}_2^n = 7.5\times 10^{-3}$ at each x bin. This in turn leads to an absolute statistical precision on d_2^n of $\Delta d_2^n \approx 1.25 \times 10^{-3}$. This value is to be compared with $\Delta d_2^n = 5\times10^{-3}$ from SLAC E155X.

The pion background was estimated using the EPC program [37] which was tested against measurements carried at JLab in a similar kinematic range. The results of the estimate are listed in Table 1 were the π/e^- ratio ranges from a negligible value in the highest x bin to a value of about twenty in the lowest x bin. Given the pion rejection performance of the Čerenkov and Lead glass calorimeter combination, we should be able to keep this correction at a negligible level. Furthermore, we shall measure the pion asymmetry using the hadron spectrometer in the lowest three x bins.

Table 1: π^-/e^- each x bin planned in this measurement

E_i (GeV)	θ_e °	E' (GeV)	x	W (GeV)	dσ^{π^-} (nb/GeV/sr)	π^- rate (Hz)	π^-/e^-
5.70	16.40	4.310	0.766	1.22	0.51	0.03	0.006
5.70	16.63	4.197	0.710	1.30	0.94	0.09	0.013
5.70	16.90	4.064	0.652	1.40	1.68	0.20	0.024
5.70	17.24	3.903	0.593	1.50	2.98	0.48	0.030
5.70	17.70	3.705	0.534	1.62	5.40	1.31	0.062
5.70	18.33	3.458	0.475	1.76	10.4	2.67	0.118
5.70	19.14	3.173	0.422	1.90	20.8	5.01	0.264
5.70	20.27	2.833	0.372	2.06	44.7	28.54	0.673
5.70	22.16	2.375	0.321	2.26	120.3	92.13	2.41
6.00	22.70	2.152	0.277	2.47	253.3	141.25	6.04
6.00	25.14	1.760	0.251	2.62	574.9	245.44	18.7

The radiative corrections (RC) will be performed in two stages. First the internal corrections will be evaluated following the procedure developed by Bardin and Shumeiko[38] for the unpolarized case and extended to the spin dependent lepto-production cross sections by Akushevish and Shumeiko[39, 40]. Second, using these internally corrected cross sections, the external corrections (for thick targets) are applied by extending the procedure developed for the unpolarized cross sections by Tsai[41, 42] with modifications appropriate for this experiment.

To evaluate the experimental systematic uncertainty of d_2^n we used relative uncertainties in the cross sections and asymmetries achieved in E94-010. Table 4 summarizes these uncertainties. One item of concern was the effect of the target relative spin misalignment between the transverse and longitudinal direction measurements. Fig. 9 shows this effect at each value of x on the integrand of d_2. A relative error of 0.5° in the relative direction of the transverse versus perpendicular results in a relative error $\Delta d_2/d_2 = 0.15\%$. Using the Weigel *et al.* [18] model of g_2 and g_1 we estimated $\Delta d_2/d_2$ to be of the order of 10 % and thus an absolute systematic uncertainty of about 10^{-3}. We believe we can achieve a relative error of 0.2° in the target spin alignment.

Even with our improved projected statistical precision the total uncertainty in d_2^n is still dominated by the statistical.

An elastic scattering asymmetry measurement is planned at low energy ($E_i = 1.0$ GeV $\theta = 17.5°$) in order to calibrate our spin dependent absolute cross sections. This quantity can be evaluated using the measured electric and magnetic form factors of ^{3}He. This measurement would actually determine the polarization of the ^{3}He nuclei along the electron beam path. False asymmetries will be checked to be consistent with zero by comparing data with target spins in opposite directions.

Also contributing to the dilution of the asymmetry is the pair-electron contamination. This correction is x dependent, and is relevant only in the lowest x region. This contamination was estimated to be no more than 6% in the worst case and will be measured in this experiment by reversing the spectrometer polarity on the right arm spectrometer.

The spectrometers cannot be used in a symmetric configuration when taking data since they don't access the same maximum range of momentum. For this reason we can only save about 456 hours using the HRS-r spectrometer and most of the large x data will be acquired using the HRS-l spectrometer. Tables 4 and 5 show the kinematics and time for each spectrometer acquiring data.

Table 2: List of the systematic error contributions to d_2^n

Item description	Subitem description	Relative uncertainty
Target polarization		4 %
Beam polarization		3 %
Asymmetry (raw)		
	• Target spin direction (0.5°)	$\approx 1.5 \times 10^{-3}$
	• Beam charge asymmetry	200 ppm
Cross section (raw)		
	• PID efficiency	$\approx$ 1 %
	• Background Rejection efficiency	$\approx$ 1 %
	• Beam charge	$<$ 1 %
	• Beam position	$<$ 1 %
	• Acceptance cut	2-3 %
	• Target density	2-3 %
	• Nitrogen dilution	2-3 %
	• Dead time	<1 %
	• Finite Acceptance cut	<1%
Radiative corrections		$\leq$ 5 %
Total effect		$\Delta d_2 \approx 5 \times 10^{-4}$
Estimate of contributions	$\int_{0.003}^{0.241} \tilde{d}_2^n \, dx$	4.8×10^{-4}
from unmeasured regions	$\int_{0.767}^{0.999} \tilde{d}_2^n \, dx$	3.9×10^{-5}
From ^{3}He to Neutron correction		5%

Table 3: Parameters per bin in (Q^2,x) plane for the proposed experiment

E_i (GeV)	bin central p (GeV)	x	Δx	Q^2 (GeV^2)	W (GeV)	Rate (Hz)	Time$_\perp$ hours	Time$_\parallel$ hours
5.70	4.31	.766	.58E-01	2.00	1.22	5.03	166.	82.2
5.70	4.20	.710	.58E-01	2.00	1.30	6.85	166.	82.2
5.70	4.06	.652	.57E-01	2.00	1.40	8.23	144.	63.7
5.70	3.90	.593	.59E-01	2.00	1.50	16.0	167.	65.5
5.70	3.71	.534	.59E-01	2.00	1.62	21.1	110.	37.4
5.70	3.46	.475	.59E-01	2.00	1.76	22.6	125	35.8
5.70	3.17	.422	.48E-01	2.00	1.90	19.0	148	35.1
5.70	2.83	.372	.52E-01	2.00	2.06	42.4	63.6	12.2
5.70	2.38	.321	.34E-01	2.00	2.26	38.1	64.9	9.4
6.00	2.15	.277	.27E-01	2.00	2.47	23.4	104	11.5
6.00	1.76	.251	.18E-01	2.00	2.61	13.1	179.	15.4

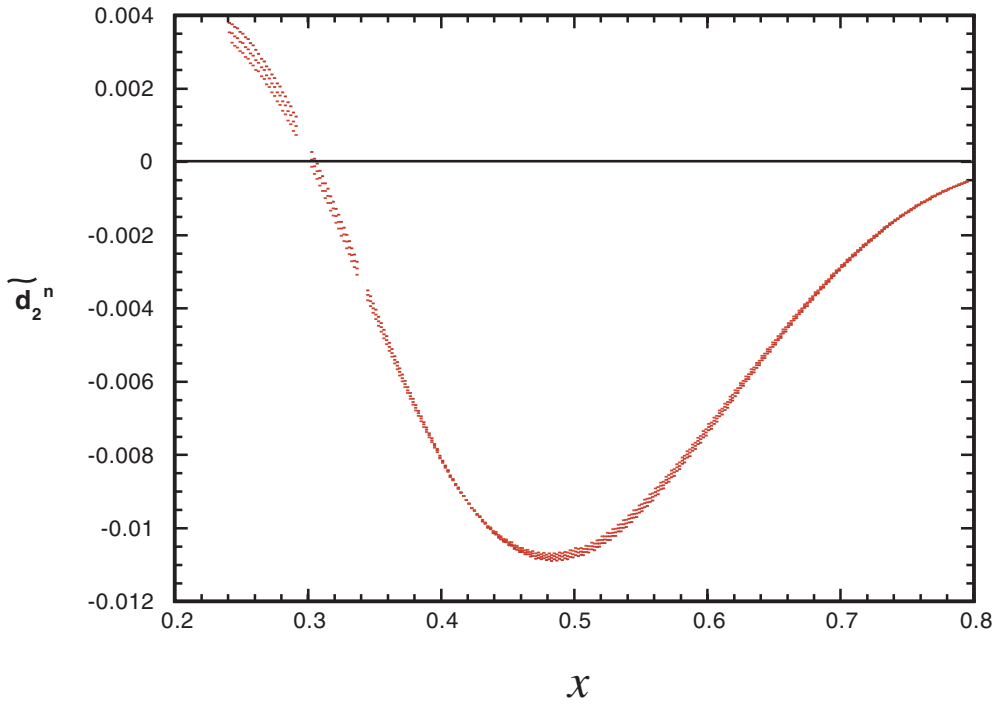

Figure 9: Effect of target relative spin misalignment by 0.5° between the transverse and longitudinal measurements

The right spectrometer will measure mainly the low x data points and will also be used to measure the positron contamination at the lowest x bins, while the HRS-l completes its measurements at large x. We will use the HRS-l for 787 hours with beam on target to complete this measurement.

5 Spin Structure Functions: From ^{3}He to the Neutron

Most of the current information on the spin-independent structure functions of the neutron comes from experiments on the deuteron. For spin-dependent structure, because the deuteron polarization is shared roughly equally between the proton and neutron, extraction of neutron spin structure functions requires a precise knowledge of the proton spin structure, in addition to the nuclear effects [43]. This problem is compounded by the fact that the spin-dependent structure functions of the proton are typically much larger than those of the neutron, making extraction of the latter especially sensitive to small uncertainties in the proton structure functions. On the other hand, since the neutron in ^{3}He carries almost 90% of the nuclear spin, polarized ^{3}He is an ideal source of polarized neutrons.

The three-nucleon system has been studied for many years, and modern three-body wave functions have been tested against a large array of observables which put rather strong constraints on the nuclear models [44]. In particular, over the past decade considerable experience has been acquired in the application of three-body wave functions to deep-inelastic scattering [45, 46, 47].

The conventional approach employed in calculating nuclear structure functions in the region $0.3 < x < 0.8$ is the impulse approximation, in which the virtual photon scatters incoherently from individual nucleons in the nucleus [48]. Corrections due to multiple scattering, NN correlations or multi-quark effects are usually confined to either the small-x ($x < 0.2$), or very large-x ($x > 0.9$)

Table 4: Sequence of measurements carried by the HRS-l spectrometer

E_i GeV	θ deg	HRS-l Central p GeV		$\text{Time}_\perp$ hours	$\text{Time}_\parallel$ hours
6.0	22.5	2.167		42.	5.7
6.0	25.0	1.756		89.5	7.7
5.7	17.5	4.069		166	82.2
5.7	17.5	3.794		167	65.5
5.7	17.5	3.538		125	35.8
			Total	589.5	196.9

Table 5: Sequence of measurements carried by the HRS-r spectrometer

E_i GeV	θ deg	HRS-r Central p GeV		$\text{Time}_\perp$ hours	$\text{Time}_\parallel$ hours
6.0	22.5	2.167		42.	5.7
6.0	25.0	1.756		89.5	7.7
5.7	20.0	3.075		148.	35.1
5.7	20.0	2.867		63.6	12.2
5.7	22.5	2.324		64.9	9.4
			Total	408	56.7

regions. In the impulse approximation the g_1 structure function of ^{3}He is obtained by folding the nucleon structure function with the nucleon momentum distribution in ^{3}He, Δf_N:

$$g_1^{^3\mathrm{He}}(x) \;=\; \int_x^3 \frac{dy}{y}\; \{2\Delta f_p(y)\; g_1^p(x/y) \;+ \Delta f_n(y)\; g_1^n(x/y)\}\,, \tag{21}$$

where y is the fraction of the ^{3}He momentum carried by the nucleon, and the dependence on scale, Q^2, has been suppressed. The nucleon momentum distributions $\Delta f_N(y)$ are calculated from the three-body nuclear wave function, which are obtained by either solving the Faddeev equation [49] or using variational methods [46], and are normalized such that:

$$\int_0^3 dy\; \Delta f_N(y) \;=\; \rho_N\;, \tag{22}$$

where ρ_N is the polarization of the nucleon in ^{3}He. While the full three-body wave function involves summing over many channels, in practice the three lowest states, namely the S, S' and D, account for over 99% of the normalization. Typically, one finds $\rho_n \approx 87\%$ and $\rho_p \approx -2\%$ [44, 45, 46, 47, 49].

The smearing in Eq.(21) incorporates the effects of Fermi motion and nuclear binding, which can become sizable at large x. Correctly accounting for these effects is important when attempting to extract information on nucleon structure functions from nuclear data at $x > 0.6$, as well as for determining higher moments of structure functions, in which the large-x region is more strongly weighted.

The nuclear corrections to the g_2^n structure function can be evaluated analogously to those for g_1^n. However, because the magnitude of g_2 is expected to be small, one could anticipate nuclear effects to play a bigger role here than in g_1^n. A difficulty in determining the size of the nuclear corrections to g_2^n is the fact that very little is known about the shape of g_2^n as a functions of x. One can estimate the order of magnitude of the possible effects by considering the twist-2 part of g_2^n, which is determined from g_1^n through the Wandzura-Wilczek relation [15] [52]:

$$g_2^{^3\mathrm{He}}(x)\Big|_{\mathrm{tw-2}} \;=\; -g_1^{^3\mathrm{He}}(x) \;+\; \int_x^3 \frac{dy}{y}\; g_1^{^3\mathrm{He}}(x/y)\;, \tag{23}$$

where $g_1^{^3\mathrm{He}}$ is given by Eq.(21).

Since the main objective of the experiment is to extract the second moment of $3g_2^n + 2g_1^n$, namely $\int dx\; x^2(3g_2^n(x) + 2g_1^n(x))$, the effects of Fermi motion at large x may be somewhat magnified.

In Fig. 10 we compare $x^2 g_2^{^3\mathrm{He}}(x)$ calculated by including the effects of Fermi smearing (dashed) and without smearing (dot-dashed) [52]. The two dashed curves correspond to the full, smeared calculation with different ^{3}He model wave functions [49, 51]. For reference the twist-2 part of the neutron g_2^n is also shown (solid). The difference in the second moments of $g_2^{^3\mathrm{He}}$ between the smearing and no-smearing cases, is again at the level of a few percent, as is the difference between the convolution results using different ^{3}He wave functions.

Although the quantitative results for g_2 cannot be viewed as definitive without also considering the twist-3 contribution, there is no reason to expect the twist-3 component to have a dramatic x-dependence so as to significantly alter the scale of the nuclear effects seen in Fig. 10.

All of the nuclear structure function analyses that have been performed instead suggest that both the neutron g_1^n and g_2^n deep-inelastic structure functions can be extracted from ^{3}He data with minimal uncertainties associated with nuclear corrections. Recently there was an investigation into the role of the $\Delta(1232)$ in deep inelastic scattering on polarized ^{3}He and how it affects the g_1 neutron spin structure function extraction [53]. The authors estimated that when taking the effect of the Δ into account the values of the first moment of g_1^n increases by $6 \div 8$ %.

Estimating all the corrections and their uncertainties we come to the conclusion that in this experiment the statistical error on the final result is still the dominant error.

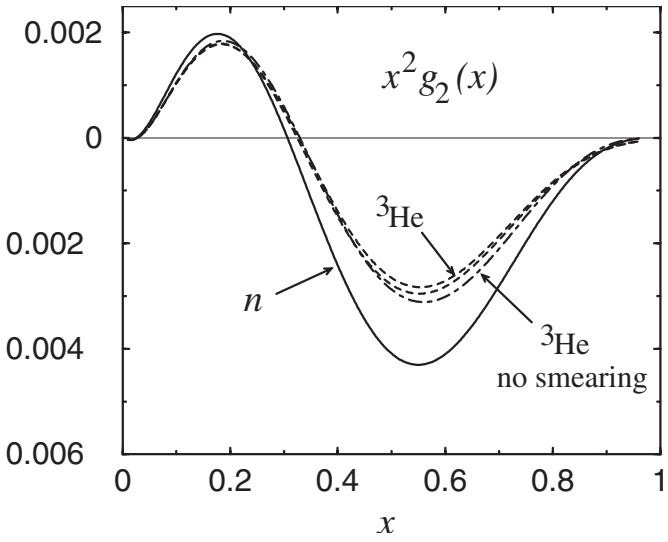

Figure 10: Structure function $x^2 g_2(x)$ for ^{3}He, calculated taking into account effects of smearing due to Fermi motion and binding, with two different model ^{3}He wave functions (dashed), and without smearing (dot-dashed) [52]. For reference the neutron structure function is also shown (solid).

6 Summary and Beam Request

In summary, we propose to carry out a precision determination of the neutron twist-three matrix element d_2^n. We will determine asymmetries in a large x region ($0.24 \leq x \leq 0.8$) (see Fig 11) from

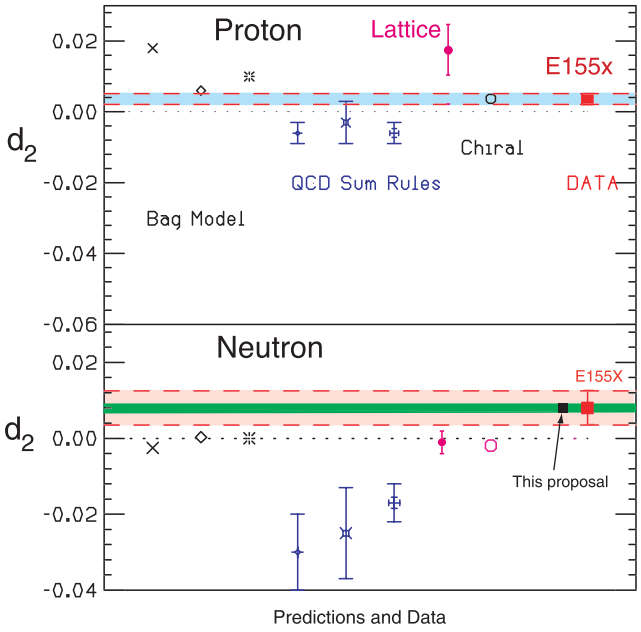

Figure 11: Same figure as Fig. 4 but with the d_2^n projected result from this proposal compared to E155X.

a measurement using a high pressure polarized ^{3}He target (P_t= 40%) and the highest available energies (5.7 and 6.0 GeV) of the polarized beam (P_b=80%). This measurement requires 589.5 hours of beam on target for the measurement of the transverse asymmetry and 197 hours for the measurement of the longitudinal asymmetry, along with 60 hours for the beam energy change, spectrometer momentum changes, elastic scattering calibration and beam and target polarization measurements. We therefore request a total of 846.5 hours (35 days) of beam time to achieve a statistical uncertainty on d_2^n of $\Delta d_2^n \approx 1.2 \times 10^{-3}$ at $Q^2 = 2.0$ GeV^2 in the measured x range.

References

[1] E. Shuryak and A. Vainshtein, Nuc. Phys. B **201** (1982) 141.

[2] R. L. Jaffe and Xiangdong Ji, Phys. Rev. D **43** (1991) 724.

[3] B. Filippone and X. Ji, hep-ph/0101224.

[4] D. Adams *et al.*, Phys. Lett. **B336** (1994) 125.

[5] P. L. Anthony *et al.*, Phys. Rev. Lett. **71** (1993) 959.

[6] P. L. Anthony *et al.*, Phys. Rev. D **54** (1996) 6620.

[7] K. Abe *et al.*, Phys. Rev. Lett. **76** (1996) 587.

[8] K. Abe *et al.*, Phys. Lett. B **404** (1997) 377.

[9] P. L. Anthony *et al.*, Phys. Lett. B**458** (1999) 529.

[10] SLAC Experiment E155X, Spokespeople: R. Arnold and J. McCarthy, (1996).

[11] (E155X) P. Bosted (for the E155X collaboration), "Very preliminary results for the spin structure function g2 from SLAC E155x", Nuc. Phys. A **666** (2000) 300c-303c

[12] X. Ji, (private communication)

[13] JLab E97-103 experiment, Spokespeople T. Averett and W. Korsh. see (http://hallaweb.jlab.org/physics/experiments/he3/g2/temp/

[14] K. Abe *et al.*, Phys. Rev. D **58** (1998) 112003-1.

[15] S. Wandzura and F. Wilczek, Phys. Lett. B **72** (1977) 195.

[16] JLab E01-012 experiment, Spokespeople N. Liyanage, J. P. Chen and S. Choi.

[17] JLab E01-006 experiment, Spokesperson O. Rondon,

[18] H. Weigel, L. Gamberg, H. Reinhart, Phys. Rev. D**55** (1997) 6910.

[19] M. Stratmann, Z. Phys. C **60** (1993) 763.

[20] X. Ji and P. Unrau, Phys. Lett. B **333** (1994) 228.

[21] X. Song, Phys. Rev. D **54** (1996) 1955.

[22] X. Ji and W. Melnitchouk, Phys. Rev. D **56** (1997) 5511.

[23] E. Stein, Phys. Lett. B **343** (1995) 369.

[24] B. Ehrnsperger, A Schäfer, Phys. Rev. D **52** (1995) 2709.

[25] I. Balitsky, V. Barun, A. Kolesnichenko, Phys. Lett. B **242** (1990) 245; B **318** (1995) 648 (E).

[26] M. Gockeler, Phys. Rev. D **53** (1996) 2317.

[27] M. Gockeler *et al.*, hep-lat/0011091.

[28] M.A. Bouchiat, T.R. Carver and C.M. Varnum, Phys. Rev. Lett. **5** (1960) 373.

[29] N.D. Bhaskar, W. Happer, and T. McClelland, Phys. Rev. Lett. **49** (1982) 25.

[30] W. Happer, E. Miron, S. Schaefer, D. Schreiber, W.A. van Wijngaarden, and X. Zeng, Phys. Rev. A **29** (1984) 3092.

[31] T.E. Chupp, M.E. Wagshul, K.P. Coulter, A.B. McDonald, and W. Happer, Phys. Rev. C **36** (1987) 2244.

[32] K.P. Coulter, A.B. McDonald, W. Happer, T. E. Chupp, and M.E. Wagshul, Nuc. Inst. Meth. in Phys. Res. **A 270** (1988) 90.

[33] N.R. Newbury, A.S. Barton, P. Bogorad, G. D. Cates, M. Gatzke, H. Mabuchi, and B. Saam, Phys. Rev. A **48** (1993) 558.

[34] K.P. Coulter, A.B. McDonald, G.D. Cates, W. Happer, T.E. Chupp, Nuc. Inst. Meth. in Phys. Res. A**276** (1989) 29 .

[35] A. Abragam, Principles of Nuclear Magnetism (Oxford University Press, New York, 1961).

[36] L. Whitlow, SLAC-report-357 (1990).

[37] J. W. Lightbody Jr. and J.S. O'Connell, Computers in Physics **2** (1988) 57.

[38] D. Yu. Bardin and N. M. Shumeiko, Nucl. Phys. B **127** (1977) 1251.

[39] T.V. Kuchto and N. M. Shumeiko, Nucl. Phys. B **219** (1983) 412.

[40] I. V. Akushevich and N. M. Shumeiko, J. Phys. **G**: Nucl. Part. Phys. **20** (1994) 513.

[41] L. W. Mo and Y. S. Tsai, Rev. Mod. Phys. **41** (1969) 205.

[42] Y. S. Tsai, SLAC-PUB-848 (1971).

[43] W. Melnitchouk, G. Piller and A.W. Thomas, Phys. Lett. B **346** (1995) 165; S. A Kulagin, W. Melnitchouk, G. Piller and W. Weise Phys. Rev. C **52** (1995) 932.

[44] J.L. Friar et al., Phys. Rev. C **42** (1990) 2310.

[45] R.M. Woloshyn, Nucl. Phys. A **496** (1989) 749.

[46] C. Ciofi degli Atti, E. Pace and G. Salme, Phys. Rev. C **46** (1992) R1591; C. Ciofi degli Atti, S. Scopetta, E. Pace, G. Salme, Phys. Rev. C **48** (1993) 968;

[47] R.W. Schulze and P.U. Sauer, Phys. Rev. C **48** (1993) 38.

[48] D.F. Geesaman, K. Saito and A.W. Thomas, Ann. Rev. Nucl. Part. Sci. **45** (1995) 337.

[49] I.R. Afnan, F. Bissey and A.W. Thomas, nucl-th/0012081..

[50] E. Leader, A.V. Sidorov and D.B. Stamenov, Int. J. Mod. Phys. A **13** (1998) 5573; Phys. Rev. D **58** (1998) 114028.

[51] I.R. Afnan, F. Bissey, J. Gomez, A.T. Katramatou, W. Melnitchouk, G.G. Petratos and A.W. Thomas, Phys. Lett. B **493** (2000) 36.

[52] F. Bissey, W. Melnitchouk, A. W. Thomas, in preparation; W. Melnitchouk, private communication.

[53] C. Boros, V. Guzey, M. Strikman, A.W. Thomas, hep-ph/0008064